The role of shape-dependent flight stability in the origin of oriented meteorites

Khunsa Amin[a,1], Jinzi Mac Huang[a,1], Kevin J. Hu[a], Jun Zhang[a,b,c], and Leif Ristroph[a,2]

[a]Applied Math Laboratory, Courant Institute, New York University, New York, NY10012; [b]New York University–East China Normal University (NYU-ECNU) Institute of Physics, New York University Shanghai, Shanghai 200062, China; and [c]Department of Physics, New York University, New York, NY 10003

The atmospheric ablation of meteoroids is a striking example of the reshaping of a solid object due to its motion through a fluid. Motivated by meteorite samples collected on Earth that suggest fixed orientation during flight—most notably the conical shape of so-called oriented meteorites—we hypothesize that such forms result from an aerodynamic stabilization of posture that may be achieved only by specific shapes. Here, we investigate this issue of flight stability in the parallel context of fluid mechanical erosion of clay bodies in flowing water, which yields shapes resembling oriented meteorites. We conduct laboratory experiments on conical objects freely moving through water and fixed within imposed flows to determine the dependence of orientational stability on shape. During free motion, slender cones undergo postural instabilities, such as inversion and tumbling, and broad or dull forms exhibit oscillatory modes, such as rocking and fluttering. Only intermediate shapes, including the stereotypical form carved by erosion, achieve stable orientation and straight flight with apex leading. We corroborate these findings with systematic measurements of torque and stability potentials across cones of varying apex angle, which furnish a complete map of equilibrium postures and their stability. By showing that the particular conical form carved in unidirectional flows is also posturally stable as a free body in flight, these results suggest a self-consistent picture for the origin of oriented meteorites.

fluid–structure interaction | flight stability | erosion | meteorite | ablation

Many important problems in the natural and engineering sciences involve the mutual influence and coupled dynamics of fluids flows with moving objects or movable boundaries (1, 2). A classic example of such fluid–structure interactions is aero- or hydroelasticity, in which a flexible object both affects and responds to an imposed flow, such as in the flapping of a flag (3–5). Other situations involve moving boundaries within flows, where the interfacial dynamics may be driven by processes such as melting, freezing, dissolving, or erosion (6–10). Particularly challenging is the reshaping of a body due its free motion through the fluid, in which case multiple couplings are at work simultaneously. An everyday example is the fluttering and tumbling of falling paper, where motion under gravity and flow-induced bending deformations arise interactively (11, 12). Other examples include the reshaping and ballooning of raindrops (13, 14), freezing or sublimation of atmospheric ice (15, 16), and the dissolution of particulates in sedimenting or stirred suspensions (17, 18).

A particularly splendid example is a meteor or "shooting star" (19, 20), which involves the hypersonic flight motions of a meteoroid that are coupled to its reshaping due to aerodynamic heating, vaporization, melting, and removal of surface material (21–24). When this process of ablation incompletely consumes a meteoroid, the resulting meteorite collected on Earth, its shape, and fusion crust of resolidified material give clues to its flight history (25–28). While most meteorites seem arbitrarily shaped and isotropically ablated, some show features that indicate a directionality of the flows responsible for sculpting the

surface, suggesting fixed posture during flight rather than tumbling (25–27). Surface features include parallel flow lines left by rivulets of molten material (29) as well as aligned regmaglypts or elongate "thumbprint" indentations (30). The portion of such samples has been reported to be about 25% (27). The most striking exhibits are intact oriented meteorites (25–27), so-called because their conical forms strongly suggest flight with apex-leading orientation. The photographs in Fig. 1 include examples from the 2013 meteor burst over Chelyabinsk, Russia (Fig. 1*A*) as well as the Adamana (Fig. 1*B*) and Karakol (Fig. 1*C*) oriented meteorites. Such conical forms have fascinated collectors and scientists alike over the last 2 centuries as documented on the website https://meteorite-recon.com.

One important question inspired by these objects is how such similar final shapes arise from the ablative sculpting of what presumably start out as arbitrarily shaped meteoroids. Much early work aimed to link the overall conical shape as well as surface features to the flows present (ref. 22 and references therein), and laboratory experiments on the ablation of plastic bodies fixed within supersonic airflow revealed the formation of a conical nose directed into the flow (32). This shape is thereafter retained as the windward face recedes. A similar convergence to a terminal shape—and a similar terminal shape itself as shown in Fig. 1*D*—have recently been observed for clay bodies undergoing fluid mechanical erosion while fixed in flowing water (31, 33). Cone shapes also result from flow-driven dissolving of salts (30). The similarity between hypersonic ablation and erosion or dissolution in fast but subsonic flows is surprising given the important differences in flow regime and in the physics of the material
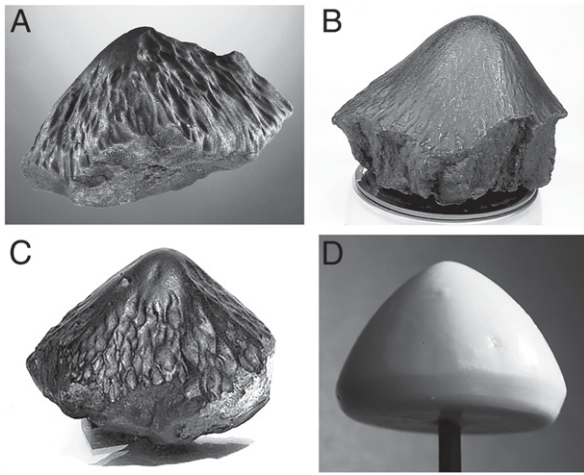
Fig. 1. Forms that result from atmospheric ablation and fluid mechanical erosion. (*A*) Oriented meteorite measuring 12 cm in width from the 2013 event over Chelyabinsk, Russia. Image courtesy of Christie's Images Limited. (*B* and *C*) Meteorites from Adamana, Arizona (15 cm wide) and Karakol, Kyrgyzstan (14 cm wide) showing similar conical forms as well as flow lines and elongated pits. Note that the lack of fusion crust on the rear surfaces suggests fragmentation, and thus, the complete shape during ablation cannot be ascertained. (*B*) Image courtesy of Marcin Cimala (photographer). (*C*) Image courtesy of Dmitry Badyukov (photographer). (*D*) Sculpting of clay by water erosion (31). An initial sphere of bentonite clay is reshaped into a cone-like form (3 cm in width), when fixed within a unidirectional flow.

removal processes. Nonetheless, these studies show quite generically that a stereotypical final form arises from the flow–solid interaction, at least when the unidirectional flow is enforced externally by fixing the body.

For a free body moving through a fluid, unidirectional flow must be achieved by fixed posture. The existence of oriented meteorites suggests aerodynamic stabilization of meteoroids during ablation: that is, the flow-induced torques tend to restore the apex-leading orientation against perturbations (25–27). While there are currently no direct observations of meteoroid orientation nor experiments on their stability in hypersonic flows, we aim to explore this hypothesis in the different but related context of eroded forms interacting with subsonic water flows. Motivated by oriented forms generally and by the parallels between hypersonic ablation and subsonic erosion, here we address the flight stability problem as relevant to the latter case through laboratory-scale experiments on conical bodies in water flows. Even at high-Reynolds number but low-Mach number conditions (34), stably oriented motion of a free body through a fluid would be somewhat surprising given the prevalence of oscillatory, tumbling, and fluttering modes exhibited by simple shapes, such as disks, plates, spheres, and cylinders (11, 35–37). The flight performance of cones has been of interest throughout the Space Age, with many stability studies carried out at high Mach numbers (38–42) and fewer under subsonic conditions (35, 43–46). However, there does not seem to be a systematic characterization of flight stability across the family of cone shapes under any flow conditions nor any general conclusions about how the cone apex angle affects stability. Varying this angle spans shapes from slender (akin to a long, thin cylinder) to broad or dull (akin to a disk), and the systematic characterization presented here for subsonic conditions allows us to assess not only the existence of stably oriented motion but also its sensitivity or robustness to changes in shape.

Our approach draws a loose analogy between the ablation of a meteoroid during its hypersonic motion through the atmosphere and the erosion of a clay object moving at subsonic speeds through water. These contexts are parallel, related in the broad

phenomenology of flow-induced reshaping but different in all details of the physics (19, 20). The value of this approach is to explore in a tractable and controlled laboratory setting a hypothesis for oriented forms: The same shape that tends to be sculpted by a unidirectional flow also satisfies the flight stability criterion needed to ensure unidirectional flow as a freely moving body. Showing this to be true in the subsonic erosion context while not directly informing meteoroid flight would lend some plausibility to the analogous explanation for oriented meteorites.

Oriented Flight of the Eroded Form

To directly assess postural stability, we first conduct experiments aimed at observing the free motions of the eroded cone-like form as well as perfect cones. Centimeter-scale solid aluminum bodies are first shaped by machining and then released to drop under gravity within a tall water tank ($30 \times 30 \times 60$ cm). Each object is released from rest without spin and with its apex directed downward, and the resulting motions are recorded from the side by a video camera. Many trials are conducted to determine the typical dynamics. To visualize the flows, additional trials are performed for the same bodies with surfaces that are thinly coated with a paste of clay and fluorescein dye. Example photographs and extracted postures are shown in Fig. 2 for a body machined to the erosion form of Fig. 1*D* (31, 33). (Note that the front surface of the eroded form is well approximated by an ogive or a surface of revolution of a circular arc.) As shown by the snapshots in Fig. 2*B*, this object falls nearly straight down with only slight lateral motions. Its apex remains closely aligned with its heading or velocity, a clear demonstration of oriented flight. This motion results in a rather straight wake flow left by the body as visualized
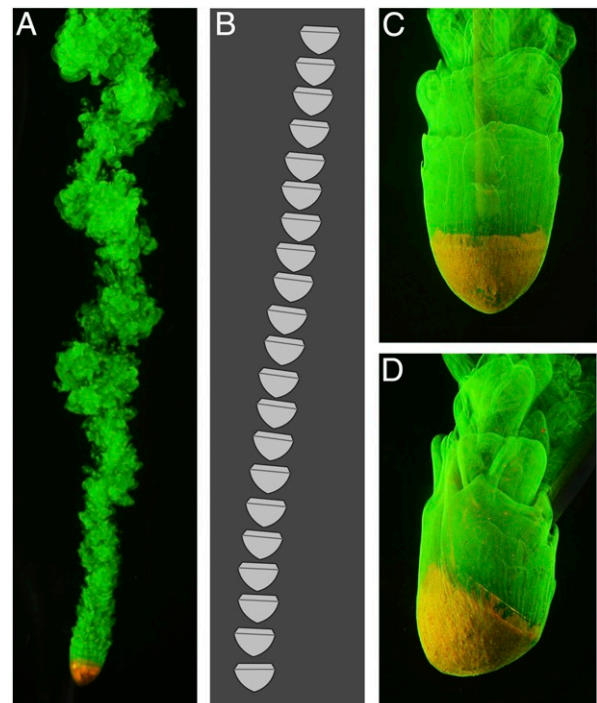
Fig. 2. Oriented flight of a body in the stereotypical shape carved by erosion. An aluminum body is machined into the eroded form of Fig. 1*D*, and its falling motions within water and associated flows are visualized. The body measures 1.2 cm at its widest diameter. (*A*) Photograph of the wake flow, which is visualized by thinly coating the body with a paste of fluorescein dye mixed with clay. (*B*) Snapshots of the posture through time for a typical descent as extracted from video. (*C*) Flow visualized by fixing the body within the laminar flow of a water tunnel. (*D*) Flow structure when misaligned to the oncoming (upward) flow.

in Fig. 2*A* by erosion of the clay-dye coating. Additional details of the near-body flow are revealed by fixing the object within the imposed flow of a water tunnel as captured by the photographs in Fig. 2 *C* and *D*. Videos of the body dynamics and wake flows are available in Movie S1.

These observations suggest that a body undergoing simultaneous motion through a fluid and erosion would, after having been sculpted into the cone-like shape, thereafter maintain the apex-leading orientation. This postural stability would ensure the unidirectional flow and flow-induced erosive shrinking that thereafter preserves this shape.

Before further exploring oriented flight, we note the relevant scales and forces: the solid bodies considered are of size $L \sim 1$ cm and density $\rho_s = 2.7$ g/cm^3, and fluid parameters are the density $\rho_f = 1.0$ g/cm^3 and kinematic viscosity $\nu = 10^{-2}$ cm^2/s of water. Balancing buoyancy-corrected weight with drag yields a scale for the resulting descent speed of $U \sim \sqrt{(\rho_s/\rho_f - 1)Lg} \sim 10 - 100$ cm/s, where $g = 980$ cm/s^2 is gravitational acceleration. The resulting Reynolds number Re $= UL/\nu \sim 10^3 - 10^4$ is high, indicating the dominance of fluid inertia over viscous effects (34).

It is also important to clarify the role of gravity or weight, which here serves to induce the descent of the body through the fluid but does not directly contribute to its orientational stability or instability. The weight acts at the center of mass and thus induces no torque about this point. A similar argument holds for buoyancy, which for a body of homogeneous density exerts no torque and acts only to modify the vertical force. The stability of posture thus depends only on the flow-induced torques about the center of mass. Thus, we expect our stability results to apply in cases where the motion is initiated by means other than gravity (e.g., for a projectile launched at high speed through a fluid).

Dynamic Flight Stability of Cones

Is oriented flight unique to the eroded form, or do many shapes show this behavior? To address this, we next consider the family of perfect cones of varying slenderness or broadness as quantified by the half-angle of the apex $\alpha \in (0°, 90°)$. Fig. 3 *A–F* shows snapshots captured from video for cones of varying α, which are selected as representative of the different behaviors observed. When released with apex aimed downward, very slender cones inevitably turn over and fall with their blunt rears leading as exemplified in Fig. 3*A* for $\alpha = 10°$. This inversion behavior suggests that the fluid torques tend to destabilize the apex-leading motion of the body. For somewhat greater α, we observe tumbling motions (Fig. 3*B*), in which the cone continually flips over and maintains no preferred orientation. At yet greater α, gliding motions (Fig. 3*C*) are seen, in which the body falls obliquely with its apex appreciably misaligned to its heading or velocity. Intriguingly, only for bodies in the approximate range $30° < \alpha < 50°$ do we see oriented flight, which is shown in Fig. 3*D* by the straight descent with apex leading for a cone of $\alpha = 35°$. For yet broader cones of $\alpha > 50°$, this stability of orientation gives way to rocking or fluttering motions (Fig. 3 *E* and *F*), in which the apex oscillates about the downward direction. Videos of these dynamics and associated wake flows are available in Movie S1.

These dynamical modes and their dependence on shape are summarized by the diagram in Fig. 3*G*. Here, the behaviors of inversion, tumbling, gliding, oriented flight, and rocking/fluttering are shown across varying α. All experimentally tested values of α are marked by circles, and the boundaries can be seen to be finely resolved. We note that bodies near such boundaries may exhibit multiple terminal behaviors (e.g., inversion and tumbling), and the categorization assigned in Fig. 3*G* is the most common terminal behavior after careful release very near the apex-down orientation. This single-parameter phase diagram shows that oriented flight is achieved only for shapes within a specific but moderately wide range of approximately $\alpha \in [30°, 50°]$, encompassing bodies that are neither too slender nor overly dull or broad.
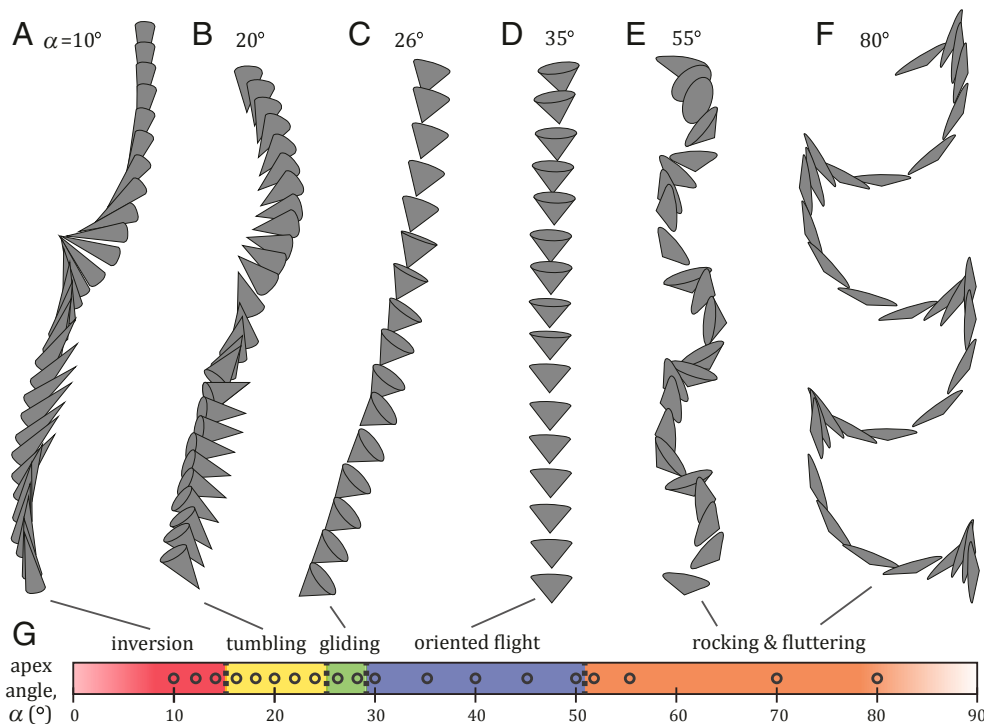
Fig. 3. Free fall dynamics of conical bodies of varying apex half-angles α. (*A–F*) Snapshots showing the descent and rotations of aluminum cones falling within water. The selected cones display the characteristic behaviors of inversion, tumbling, gliding, oriented flight, rocking, and fluttering. (*G*) Single-parameter phase diagram for flight modes across $\alpha \in (0°, 90°)$. Circles represent all cones tested in this study, and modes are color coded.

Amin et al.

Torque Measurements and Static Stability

To better understand the basis for these dynamic behaviors, we conduct static stability tests, in which cone and cone-like bodies are fixed within an imposed flow and the fluidic torques are measured as a function of orientation. For each trial, a plastic body is 3D printed and mounted to a Cavendish-style torsion balance that sits atop the test section of a laminar flow water tunnel as shown in Fig. 4A. Flow-induced torque loads a torsional spring that leads to slight rotation ($< 2°$), which is amplified for measurement using a reflected laser beam of long path length (47, 48). Calibration with known loading yields the torque N, which is measured for each body and at varying orientation angle θ relative to the incoming flow of speed U (Fig. 4B). Care is taken to mount each body through its center of mass (located 1/4 from base to apex for a solid cone), ensuring that the measurement reflects only fluid dynamical torques about this point. For the results presented here, we use bodies of somewhat larger scale $L \sim 5$ cm in flows of slower speed $U = 12.5$ cm/s, yielding similarly high Reynolds numbers $\mathrm{Re} \sim 10^3 - 10^4$.

To compare the torque orientation profile across different shapes, we consider the torque coefficient C_N, which normalizes the measured N by $\rho_f U^2 V / 2$, where V is the volume of the body. This nondimensionalization removes the expected scaling with fluid density, flow speed, and body size based on high-Re pressure forces (34), thus highlighting the effect of shape for bodies of equal volume. The plot of Fig. 4C compares the profiles $C_N(\theta)$ for the erosion form (Fig. 4C, black curve) of Fig. 1D and for cones of varying α (Fig. 4C, colors). For clarity, these same data are also broken down according to the observed dynamical modes in the plots of Fig. 4 D–G.

As an example, the erosion form yields the $C_N(\theta)$ profile shown as the black curves in Fig. 4 C and F. Orientations of $\theta = 0°$ and $\theta = 180°$ correspond to the apex aimed forward into the flow and backward away from the flow, respectively, and we see both yield $N = 0$. These orientations thus correspond to equilibrium postures as one expects given the axisymmetric shape. A nontrivial equilibrium is also found near $\theta = 115°$. The stability of each equilibrium posture can be inferred from the local slope

of the $N(\theta)$ curve (49). For example, the slope is negative near $\theta = 0°$, meaning that perturbations that increase θ are resisted by negative N, while decreasing θ is countered by positive N. The fluidic torque acts as a Hookean torsional spring $N \sim -\theta$, where the negative slope implies stability. Thus, for the erosion form, the apex-leading motion of $\theta = 0°$ is statically stable as is the backward orientation $\theta = 180°$. The $\theta \approx 115°$ equilibrium posture is unstable, since increasing (or decreasing) θ is exacerbated by increasing (or decreasing) N. In addition to corroborating the stability of $\theta = 0°$ for the eroded form, these data show that all perturbations of $0° < \theta < 115°$ are resisted by $N < 0$, tending to rotate the body back to $\theta = 0°$. The apex-leading motion thus has a robust stability with a broad basin of attraction.

How does the stability of $\theta = 0°$ depend on shape? To address this generally, we again examine the family of cones of differing half-angle α. As shown in Fig. 4D, slender bodies that display inversion during free fall have positive N for all $0° < \theta < 180°$, implying instability of $\theta = 0°$ and stability of $\theta = 180°$. This is consistent with these bodies' apex-up descent observed in free flight. As shown in Fig. 4E, cones that tend to tumble or glide have 4 equilibria, with a new stable–unstable pair appearing for intermediate θ. As shown in Fig. 4F, bodies that display stably oriented flight have only 3 equilibria, and the $\theta = 0°$ posture has now become stable. This is consistent with the maintenance of apex-leading posture seen by these bodies during free fall. As shown in Fig. 4G, the broad or dull cones that undergo rocking or fluttering have qualitatively similar profiles, with stable equilibria at $\theta = 0°$ and $180°$ and an unstable posture at intermediate $\theta \approx 90° - 100°$. These profiles differ from those of the oriented flyers in that C_N tends to be larger.

The postural equilibria and their stability are organized by the map in Fig. 5, where stable or attracting orientations (black circles) and unstable or repelling orientations (white circles) are shown for cones of varying α. The background color represents the stability potential defined as $P(\theta) = -\int_0^\theta C_N(\theta') \mathrm{d}\theta'$, which is a dimensionless measure of the potential energy associated with rotation of a body given its torque profile. Potential curves are computed from $C_N(\theta)$ for cones of α values indicated by the markers, and these data are interpolated to generate the map.
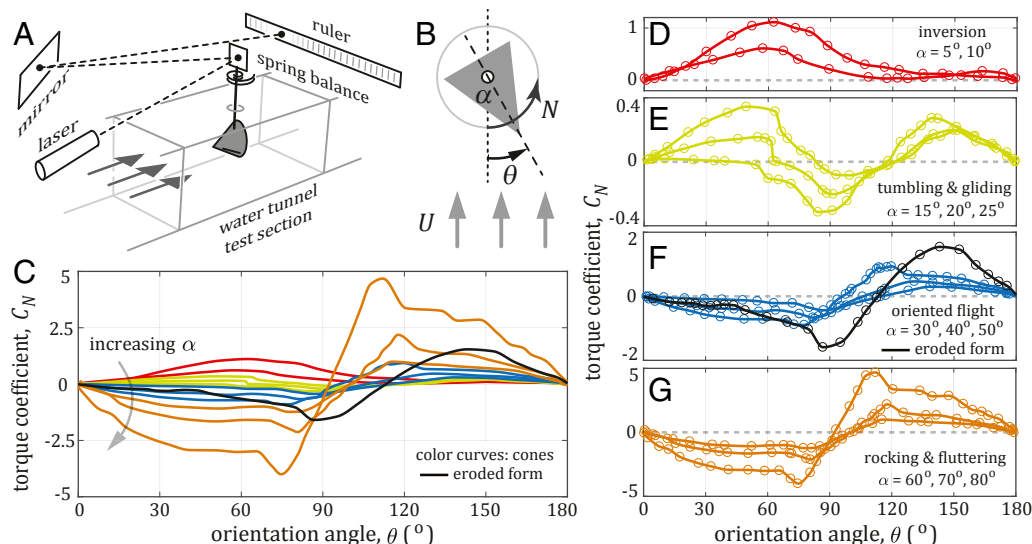
Fig. 4. Static stability of cones fixed in a unidirectional flow. (A) Apparatus for measuring torque on a body fixed at different orientations in a laminar flow of water. A spring balance sits atop the test section of a water tunnel, and torque-induced rotations of the body are amplified optically for measurement. (B) The torque N is measured across orientation angles θ for each cone of half-angle α. (C) Torque coefficient $C_N = 2N/\rho_f U^2 V$ across θ for cones (colored curves) and the eroded form (black). Here, $\rho_f = 1.0$ g/cm^3 is the density of water, $U = 12.5$ cm/s is the flow speed, and V is the volume of each body. (D–G) Torque profiles $C_N(\theta)$ separated according to free fall behaviors of inversion (red), tumbling/gliding (yellow-green), oriented flight (blue), and rocking/fluttering (orange). Measurement errors are smaller than the symbol size.

Amin et al.

The evolution of θ can be viewed as tending to lower P. For example, a cone of small $\alpha < 12°$ released at any initial orientation will tend to progress toward $\theta = 180°$, which is the minimum of a potential valley or well. This is consistent with the inversion of slender cones during free fall. Cones of $12° < \alpha < 28°$ have 2 minima and 2 maxima of P, but the variations in the potential landscape are weak. Tumbling during free fall for some such cones may be explained by the lack of any strongly preferred orientation. For $\alpha > 28°$, the stable postures of $\theta = 0°$ and $\theta = 180°$ correspond to valleys of P that are separated by a branch of unstable equilibria lying along an elevated ridge. In free fall, these bodies either converge to $\theta = 0°$ and thus, display oriented flight or oscillate within the valley and display rocking or fluttering.

Viewing the map of Fig. 5 as a whole, the stable (Fig. 5, solid curves) and unstable (Fig. 5, dashed curves) branches reveal the intricate dependence of flight dynamics on body shape, parametrized here by α. Inversion gives way to tumbling via a blue sky or saddle-node bifurcation (50) near $\alpha = 12°$, in which a stable–unstable pair of equilibria is born. Gliding gives way to oriented flight via a pitchfork bifurcation (50) near $\alpha = 28°$, in which stable branches are destroyed and the $\theta = 0°$ branch transitions from unstable to stable.

Discussion and Conclusions

The static and dynamic stability studies presented here help to rationalize the role of shape in achieving oriented flight under high speed but subsonic conditions. To relate the results of these 2 types of tests, it is important to note that static stability is a necessary but not sufficient condition for dynamic stability. In light of Fig. 5, all sufficiently broad bodies of $\alpha > 30°$ experience restoring torques when forward facing, and our free flight or dynamic tests on perfect cones show that in fact only bodies of half-angle $30° < \alpha < 50°$ achieve stably oriented flight. The eroded form of Fig. 1D does so as well, indicating that this stability is not particularly sensitive to geometric details. These results point to a cone of intermediate breadth and homogeneous density as a surprisingly simple solution to the problem of stabilizing flight.

In comparing with the previous literature, we are aware of one subsonic study on the dynamic stability of cones at comparable Re that noted the stability of apex-leading descent, although

for a somewhat smaller range of $30° < \alpha < 40°$ and limited to $Re < 10^3$ (35). At higher Mach numbers, there is a vast literature on various shapes with conical forebodies (38–42), but different methods have led to conflicting conclusions regarding the dependence of stability on cone angle (41). Furthermore, there does not seem to be a systematic study across the family of cones or any general conclusions regarding the apex angle (41). For subsonic conditions, future studies might explore a broader range of Re and assess the modes as a function of this and the other relevant dimensionless parameters of ρ_s/ρ_f and α. The basic mechanisms for how fluidic forces are redistributed to restore the apex-leading orientation in the face of perturbations and how oscillations are damped also remain to be investigated. Nevertheless, our characterization of flight stability across the family of cones could prove applicable to a variety of problems in which shape effects are important, such as the atmospheric motions of hail and other so-called hydrometeors (15, 16) as well as particulate dynamics in chemical engineering applications (51, 52).

Regarding oriented forms, it is striking that the meteorites in Fig. 1 A–C share the same basic shape as the conical forms that achieve oriented flight in our experiments. While we are not aware of quantitative characterizations of meteorite shapes, inspection of such photographs shows that oriented forms are approximately conical with apex half-angles of $40° − 50°$. Furthermore, supersonic ablation experiments have yielded nose cones of $\alpha \approx 40°$ (32), and experimental and theoretical work associates $50°$ with boundary-layer reattachment (22). The similarity of such angles to that of the cone carved in our erosion experiments (Fig. 1D) should be viewed as coincidental given the distinct meteor phenomena of hypersonic entry, shock formation, thermodynamic effects associated with ablative mass loss, fragmentation, and slowing and cooling during the so-called dark flight before ground impact (19, 20, 23, 24, 53, 54). The more intriguing coincidence revealed by our work on erosion is that the particular shape that tends to be carved for bodies fixed in unidirectional flows (31) also satisfies the postural stability criterion needed to ensure unidirectional flow as a free body (i.e., oriented flight). The conical form that "solves" the reshaping problem also solves the orientation problem. This is surprising given that the 2 problems involve distinct physical mechanisms, with erosion driven by skin friction or shear stresses and torques dominated by pressure stresses (31, 33). At the same time, this finding lends some plausibility to the same coincidence being behind the explanation for oriented meteorites. Self-stability of posture would account for the unidirectionality of flow that gives conical meteorites their characteristic shape and surface morphologies.

For both subsonic erosion and hypersonic ablation, it remains unresolved how oriented forms result from the reshaping and reorientation processes that occur simultaneously and interactively during flight. Said informally, there seems to be a "chicken-and-egg problem." An erodible body is carved into a cone-like form if held at fixed orientation (31), and we now know that a free body of this fixed shape achieves aerodynamically stabilized orientation, but which process happens first? Which is cause, and which is effect? Although this issue is challenging to address for meteoroids, different hypotheses could be studied in the subsonic regime through laboratory experiments on free and erodible bodies held aloft against gravity in an upward flow of water. The shape-dependent stability results presented here can be understood as indicating the postural dynamics that one expects as the shape-changing object proceeds through different morphologies. In particular, if the free object is to reach the terminal conical form and thereafter self-similarly shrink, then it seems necessary that this shape be posturally stable.

While the complete origin story of oriented meteorites is yet to be told, we should now more deeply appreciate these curious objects whose arrival on Earth seems possible only because of a
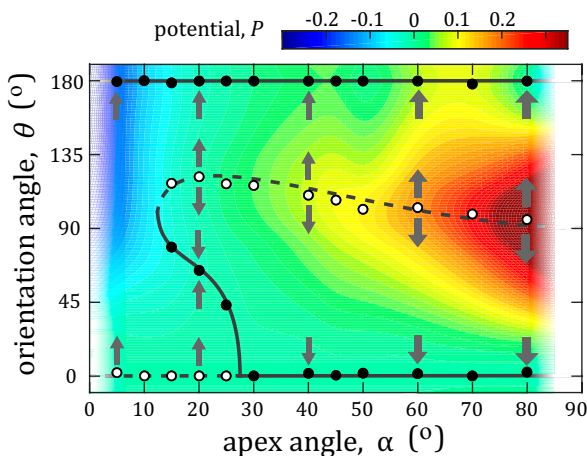

Fig. 5. Map of equilibrium orientation angles and their stability across cone shapes. For each cone of apex half-angle α, the measured stable or attracting (black circles) and unstable or repelling (white circles) orientation angles θ are shown. The color map indicates the dimensionless stability potential, $P(\theta) = -\int_0^\theta C_N(\theta')d\theta'$, which is computed for the marked α values and interpolated elsewhere.

concurrence and apparent coincidence of 2 dynamic stabilities. The same conical form seems to represent the stable solution both to the ablative reshaping of a body by the atmosphere and to the aerodynamic stabilization of posture during motion through it.

Materials and Methods

The custom-made torque balance consists of a shaft that is mounted vertically via a housing fixture to the lid of a water tunnel (Engineering Laboratory Design, Inc.). The housing connects to the shaft via a pair of low-friction ball bearings that allow rotation, and a torsional spring connecting the shaft to the housing is loaded by any applied torque. Three-dimensionally printed bodies are attached to the lower end of the shaft that sits near the middle of the tunnel test section. Bodies may be attached at any orientation angle θ relative to the flow direction. Calibration is carried out by affixing to the upper end of the shaft a horizontal rod to which a thread is tied. This thread is made to hang over a pulley, and known weights are added, loading the spring and yielding corresponding displacements of the laser beam that reflect off a shaft-mounted mirror. This procedure yields a torque displacement conversion factor of 4.64 dyn·cm/mm that is applied to all displacement data measured for different bodies at varying θ.

1. E. H. Dowell, K. C. Hall, Modeling of fluid-structure interaction. *Annu. Rev. Fluid Mech.* **33**, 445–490 (2001).
2. M. J. Shelley, J. Zhang, Flapping and bending bodies interacting with fluid flows. *Annu. Rev. Fluid. Mech.* **43**, 449–465 (2011).
3. J. Zhang, S. Childress, A. Libchaber, M. Shelley, Flexible filaments in a flowing soap film as a model for one-dimensional flags in a two-dimensional wind. *Nature* **408**, 835–839 (2000).
4. M. Argentina, L. Mahadevan, Fluid-flow-induced flutter of a flag. *Proc. Natl. Acad. Sci. U.S.A.* **102**, 1829–1834 (2005).
5. Y. C. Fung, *An Introduction to the Theory of Aeroelasticity* (Courier Dover Publications, 2008).
6. J. Crank, *Free and Moving Boundary Problems* (Oxford Science Publications, 1987).
7. J. M. Huang, M. N. J. Moore, L. Ristroph, Shape dynamics and scaling laws for a body dissolving in fluid flow. *J. Fluid Mech.* **765**, R3 (2015).
8. M. N. J. Moore, Riemann-hilbert problems for the shapes formed by bodies dissolving, melting, and eroding in fluid flows. *Commun. Pure Appl. Math.* **70**, 1810–1831 (2017).
9. W. H. Mitchell, S. E. Spagnolie, A generalized traction integral equation for Stokes flow, with applications to near-wall particle mobility and viscous erosion. *J. Comput. Phys.* **333**, 462–482 (2017).
10. L. Ristroph, Sculpting with flow. *J. Fluid Mech.* **838**, 1–4 (2018).
11. U. Pesavento, Z. J. Wang, Falling paper: Navier-Stokes solutions, model of fluid forces, and center of mass elevation. *Phys. Rev. Lett.* **93**, 144501 (2004).
12. D. Tam, J. W. M. Bush, M. Robitaille, A. Kudrolli, Tumbling dynamics of passive flexible wings. *Phys. Rev. Lett.* **104**, 184504 (2010).
13. H. R. Pruppacher, K. V. Beard, A wind tunnel investigation of the internal circulation and shape of water drops falling at terminal velocity in air. *Q. J. R. Meteorol. Soc.* **96**, 247–256 (1970).
14. A. Wierzba, K. Takayama, Experimental investigation of the aerodynamic breakup of liquid drops. *AIAA J.* **26**, 1329–1335 (1988).
15. C. A. Knight, N. C. Knight, Conical graupel. *J. Atmos. Sci.* **30**, 118–124 (1973).
16. J. P. Böhm, Review of flow characteristics and kinematics of hydrometeors in free fall. *Atmos. Res.* **26**, 285–302 (1991).
17. V. G. Levich, *Physicochemical Hydrodynamics* (Prentice Hall, 1962).
18. T. J. Hanratty, Stability of surfaces that are dissolving or being formed by convective diffusion. *Annu. Rev. Fluid. Mech.* **13**, 231–252 (1981).
19. Z. Ceplecha *et al.*, Meteor phenomena and bodies. *Space Sci. Rev.* **84**, 327–471 (1998).
20. V. A. Bronshten, *Physics of Meteoric Phenomena* (Springer, 2012), vol. 22.
21. B. Baldwin, Y. Sheaffer, Ablation and breakup of large meteoroids during atmospheric entry. *J. Geophys. Res.* **76**, 4653–4668 (1971).
22. V. A. Bronshten, "Ablation of meteoroids" in Physics of Meteoric Phenomena (D. Reidel Publishing Company, Dordrecht, 1983), pp. 91–138.
23. E. J. Opik, *Physics of Meteor Flight in the Atmosphere* (Courier Corporation, 2004).
24. O. Popova, Meteoroid ablation models. *Earth Moon Planets* **95**, 303–319 (2004).
25. V. F. Buchwald, *Handbook of Iron Meteorites: Their History, Distribution, Composition, and Structure* (State University, Center for Meteorite Studies, and Berkeley: University of California Press, 1975), vol. 1–3.
26. F. Heide, F. Wlotzka, "The meteorites" in *The Meteorites: Messengers from Space* (Springer, Berlin, 1995), pp. 97–168.
27. O. R. Norton, *The Cambridge Encyclopedia of Meteorites* (Cambridge Univ Press, Cambridge, UK, 2002).
28. J. T. Wasson, *Meteorites: Classification and Properties* (Springer Science & Business Media, 2012), vol. 10.
29. S. Feldman, On the instability theory of the melted surface of an ablating body when entering the atmosphere. *J. Fluid Mech.* **6**, 131–155 (1959).
30. D. T. Williams, A fluid-dynamic mechanism of meteorite pitting. *Smithson. Contrib. Astrophys.* **3**, 46–67 (1959).
31. L. Ristroph, M. N. J. Moore, S. Childress, M. J. Shelley, J. Zhang, Sculpting of an erodible body by flowing water. *Proc. Natl. Acad. Sci. U.S.A.* **109**, 19606–19609 (2012).
32. V. N. Kalashnik *et al.*, On the shape of bodies ablating in a supersonic gas stream. *Fluid Dyn.* **16**, 11–14 (1981).
33. M. N. J. Moore, L. Ristroph, S. Childress, J. Zhang, M. J. Shelley, Self-similar evolution of a body eroding in a fluid flow. *Phys. Fluids* **25**, 116602 (2013).
34. D. J. Tritton, *Physical Fluid Dynamics* (Springer Science & Business Media, 2012).
35. K. O. L. F. Jayaweera, B. J. Mason, The behaviour of freely falling cylinders and cones in a viscous fluid. *J. Fluid Mech.* **22**, 709–720 (1965).
36. S. B. Field, M. Klaus, M. G. Moore, F. Nori, Chaotic dynamics of falling disks. *Nature* **388**, 252–254 (1997).
37. P. Ern, F. Risso, D. Fabre, J. Magnaudet, Wake-induced oscillatory paths of bodies freely rising or falling in fluids. *Annu. Rev. Fluid. Mech.* **44**, 97–121 (2012).
38. J. Brady, Z. J. Levensteins, W. C. Lyons, Hypersonic drag, stability, and wake data for cones and spheres. *AIAA J.* **2**, 1948–1955 (1964).
39. A. N. Madagan, C. J. Welsh, G. L. Winchenbach, Free-flight investigation of the aerodynamic characteristics of a cone at high mach numbers. *AIAA J.* **8**, 294–300 (1970).
40. H. Lewis, R. East, "Measurement of free-flight dynamic stability derivatives of cones in a hypersonic gun tunnel" in *International Aerospace Planes and Hypersonics Technologies*, 10.2514/6.1995-6082.
41. C. D. Kazemba, R. D. Braun, I. G. Clark, M. Schoenenberger, Survey of blunt-body supersonic dynamic stability. *J. Spacecr. Rockets* **54**, 109–127 (2016).
42. J. E. Johnson, R. P. Starkey, M. J. Lewis, Aerodynamic stability of reentry heat shield shapes for a crew exploration vehicle. *J. Spacecr. Rockets* **43**, 721–730 (2006).
43. J. R. Calvert, Experiments on the low-speed flow past cones. *J. Fluid Mech.* **27**, 273–289 (1967).
44. M. K. Sharma, R. P. Chhabra, An experimental study of free fall of cones in Newtonian and non-Newtonian media: Drag coefficient and wall effects. *Chem. Eng. Process. Process Intensif.* **30**, 61–67 (1991).
45. A. Borah, R. P. Chhabra, Drag on freely falling cones in Newtonian and in power law fluids. *Can. J. Chem. Eng.* **83**, 559–565 (2005).
46. A. M. Hamed, Y. Jin, L. P. Chamorro, On the transient dynamics of the wake and trajectory of free falling cones with various apex angles. *Exp. Fluids* **56**, 207 (2015).
47. S. Alben, M. Shelley, J. Zhang, Drag reduction through self-similar bending of a flexible body. *Nature* **420**, 479–481 (2002).
48. L. Ristroph, J. Zhang, Anomalous hydrodynamic drafting of interacting flapping flags. *Phys. Rev. Lett.* **101**, 194502 (2008).
49. J. B. Marion, *Classical Dynamics of Particles and Systems* (Academic Press, 2013).
50. S. H. Strogatz, *Nonlinear Dynamics and Chaos: With Applications to Physics, Biology, Chemistry, and Engineering* (CRC Press, 2018).
51. C. Bernhardt. Sedimentation of nonspherical particles. *Part Syst Charact.* **8**, 209–214 (1991).
52. R. Darby, *Chemical Engineering Fluid Mechanics* (CRC Press, 2001).
53. E. A. Silber, M. Boslough, W. K. Hocking, M. Gritsevich, R. W. Whitaker, Physics of meteor generated shock waves in the earth's atmosphere–a review. *Adv. Space Res.* **62**, 489–532 (2018).
54. M. E. Tabetah, H. J. Melosh, Air penetration enhances fragmentation of entering meteoroids. *Meteorit. Planet. Sci.* **53**, 493–504 (2018).